Surfactant-induced adsorption and self-organization of particles at the air-water interface: toward a simple route for two-dimensional colloidal crystallization

Manos Anyfantakis[1,2,3]†*, Jacopo Vialetto[1,2]†, Andreas Best[4], Günter K. Auernhammer[4], Hans-Jürgen Butt[4], Bernard P. Binks[5], and Damien Baigl[1,2]*

[1]*École Normale Supérieure, PSL Research University, UPMC Univ Paris 06, CNRS, Department of Chemistry, PASTEUR, 24 rue Lhomond, 75005 Paris, France*

[2]*Sorbonne Universités, UPMC Univ Paris 06, ENS, CNRS, PASTEUR, 75005 Paris, France*

[3]*University of Luxembourg, Physics & Materials Science Research Unit, 162a Avenue de la Faiencerie, Luxembourg L-1511, Luxembourg*

[4]*Max Planck Institute for Polymer Research, Ackermannweg 10, 55128 Mainz, Germany*

[5]*School of Mathematics and Physical Sciences, University of Hull, Hull, HU6 7RX, U.K.*

†These authors contributed equally to the work.

Correspondence to: anyfas.com@gmail.com, damien.baigl@ens.fr

Abstract

To be added at the very end…

Introduction

Controlling the adsorption of particles at a fluid interface and their organization in two-dimensions is a crucial process (1) that is directly involved in numerous industrial, environmental and technological applications (2, 3). From a fundamental viewpoint, particles at interfaces also provide both a rich playground for studying physical phenomena at two dimensions (4) and an invaluable technological platform for the development of functional materials with tunable properties (5). However, the intricate multi-scale nature of the underlying physico-chemical components on the one hand challenges our current understanding (6) and, on the other hand, hinders the broad applicability of this otherwise high-potential platform (7).

In this study, we describe a new and remarkably simple way to induce particle adsorption at an air-water interface and further control their 2D organization. We show that, when a minute amount of cationic surfactant is added to a dilute aqueous suspension of anionic microparticles contained in small chamber, a significant amount of the particles is adsorbed to the air-water interface. Depending on the particle and/or the surfactant concentration, the adsorbed particles are organized in various two-dimensional structures, from close-packed colloidal crystals to loosely packed gels. Taking advantage of its simplicity, we utilize this experiment as a simple platform to investigate and explain i) how surfactants induce the adsorption of the particles to the interface and ii) how the particle as well as the surfactant concentration mediate the interparticle attractions and thus the structure of the formed monolayer.

Our experiments qualitatively differ from what has been reported so far regarding the self-assembly of colloidal particles at a fluid interface in two dimensions, in the following aspects. First, the microparticles are directly adsorbed from the bulk of the suspension to the air-water interface. This is in contrast to most studies, where a small amount of a particle suspension in a water- immiscible organic solvent is spread on the water surface, forcing the particles to stay at the air-water interface after the evaporation of the organic solvent (3). This spreading methodology has been widely used to study the behavior of particle monolayers at the air-water interface, especially during compression or expansion in Langmuir troughs (8). Second, oppositely charged surfactants have been extensively exploited to alter the surface properties of particles and therefore to mediate their interaction with a fluid interface (9). More specifically, surfactants at high enough concentrations were found to adsorb on the charged and hydrophilic particles via electrostatic and hydrophobic interactions and alter their wettability. At the surfactant concentration regime where particles became hydrophobic, they could then adsorb to the air-water interface (10). This very efficient approach has been exploited to stabilize foams (11) and emulsions (12), or for other applications, such as the suppression of the coffee-ring effect (13, 14). However, due to the fact that particles become almost neutral upon surfactant adsorption, they become barely repulsive and thus poorly prone to crystallization.

Here, for the first time, we demonstrate that a very small amount of a cationic surfactant is enough to induce the adsorption of negatively charged particles to the air-water interface. At these concentrations, which are typically four orders of magnitude lower than the critical micellar concentration, surface tension effects are negligible. By means of zeta potential measurements we confirm that there is no significant surfactant adsorption on the particle surface, thus enabling the adsorbed particles, which maintained most of their initial charge, to organize and eventually crystallize at the interface. We suggest that it is the preferential adsorption of the surfactants at the air-water interface that diminishes the electrostatic barrier and therefore facilitates the adsorption of anionic particles there (15). To our knowledge, such an “electrostatic shielding” effect, which is reminiscent to the role of salts in mediating particle adsorption at the air-water interface (15–17), has never been described using surfactants. A striking advantage of surfactants over simple salts is their inherent ability to accumulate at the interface, therefore strongly increasing their shielding efficiency. As a result, we show that particle adsorption and crystallization can be induced at micromolar concentrations of surfactant, which are at least three orders of magnitude smaller than typical electrolyte concentrations used to promote particle adsorption. In this paper, we describe two ways to induce the adsorption of anionic particles at the air-water interface, using a very small concentration of cationic surfactants in a regime where their adsorption on particles and effects on surface tension are insignificant. Through a combination of optical and confocal microscopy, we explain how both surfactant and particle concentration control the way particles organize at the interface. We established a phase diagram evidencing a wide range of conditions where extended two-dimensional colloidal crystals can be obtained in fully reproducible way. Finally, we demonstrate that this same principle can be applied to crystallize two inherently different types of microparticles (polystyrene and silica), suggesting that it is operational irrespective of the exact physicochemical particle properties. Overall, our findings provide both a new look at particle behavior at fluid interfaces and a useful guideline for the design of functional two-dimensional materials in a robust, simple and cost-effective way.

Experimental results and discussion

Particle adsorption and two-dimensional organization at the liquid-gas interface

A schematic representation of our experiment is shown in Fig. 1. We mixed a dilute aqueous suspension of anionic polystyrene (PS) microparticles (diameter 5.1 µm, carboxyl and sulfate surface groups) with an aqueous solution of cationic surfactant dodecyltrimethylammonium bromide (DTAB) in an Eppendorf tube. The concentration of microparticles and surfactants in the final mixture was C_p = 5 mg/mL and C_s = 10 µM, respectively. We transferred 200 µL of the mixture to a cylindrical (diameter 7 mm) chamber made of polystyrene by means of a micropipette, and we placed a glass coverslip on the chamber to prevent water evaporation. The sample was placed on the stage of an upright microscope, and was left unmoved overnight at room temperature. Inspection of the sample with brightfield transmission microscopy revealed that, whereas most of the microparticles were placed at the bottom of the chamber due to sedimentation, a significant amount of particles were adsorbed to the liquid-gas (LG) interface. These interfacial particles formed a two-dimensional (2D) colloidal crystal at the center of the LG interface, *i.e.* at the middle of the chamber (Fig. 1A, i and ii). We hypothesized that DTAB was responsible for promoting the adsorption of particles to the LG interface and their subsequent crystallization. To test this hypothesis, we repeated the same experiment in pure water and we found that, in the absence of surfactants, almost no particles were adsorbed at the air-water interface (Fig. 1 A, ii).

We attributed the transport of the particles to the free interface of the particle/surfactant mixture to convection. Flow visualization experiments revealed that convection was always present in our samples, presumably due to unavoidable small variations in ambient temperature (in the order of ~ 0.1 ^{o}C). We hence devised a simple method to realize a controlled transport mechanism that would bring particles to the LG interface in a reproducible fashion. After loading the chamber with our surfactant/particle mixture, we inverted the chamber and let it in this position for two hours. Note that the capillary forces prevented the liquid to flow out of the chamber. We kept the surfactant concentration the same as for the direct experiment (C_s = 10 µM), however we employed much lower particle concentration, C_p = 0.05 mg/mL. We chose this C_p because i) it should yield a surface coverage similar to the that in the direct experiments (assuming that all particles adsorb to the free interface) and ii) the absence of sedimented particles at the bottom of the chamber would allow for better transmission imaging due to the absence of strong scattering. After the two-hour time period, we inverted the chamber once again and hence brought it to its initial position (Fig. 1B, i). Similar to the direct experiment, we observed a two-dimensional polycrystalline patch of circular shape, having a diameter of about 1.62 mm. A representative movie of this inverse experiment is provided in the Supporting Information (Movie S2). A control experiment using the same colloidal suspension but without surfactants (C_s = 0 mM), yielded no particle adsorption at the LG interface, and thus no 2D structure was formed (Figure 1B, ii). We conducted further experiments mixing the PS suspensions with anionic (sodiumdodecyl sulfate, Fig. S1) or non-ionic surfactants (triethoxy monooctylether, Fig. S2), and we found that almost no particles were adsorbed at the interface. All these findings indicate that, regardless of the exact particle concentration, a very low amount of DTAB molecules (in the order of µM) induced the adsorption of particles to the air-water interface. Once adsorbed, these particles were subsequently self-organized into a two-dimensional interfacial colloidal crystal.

~~In Movie S2 we show the crystallization process. The particles collect in the centre of the chamber during a period of about 6 hours. During this time, the first aggregate formed is not crystalline; a minimum number of particles in the aggregate at the interface is required to promote their collective crystallization. Once the critical number of particles is reached, the structure crystallizes from his centre, in several domains containing few vacancies and defects, up to around 68% of his total area.~~

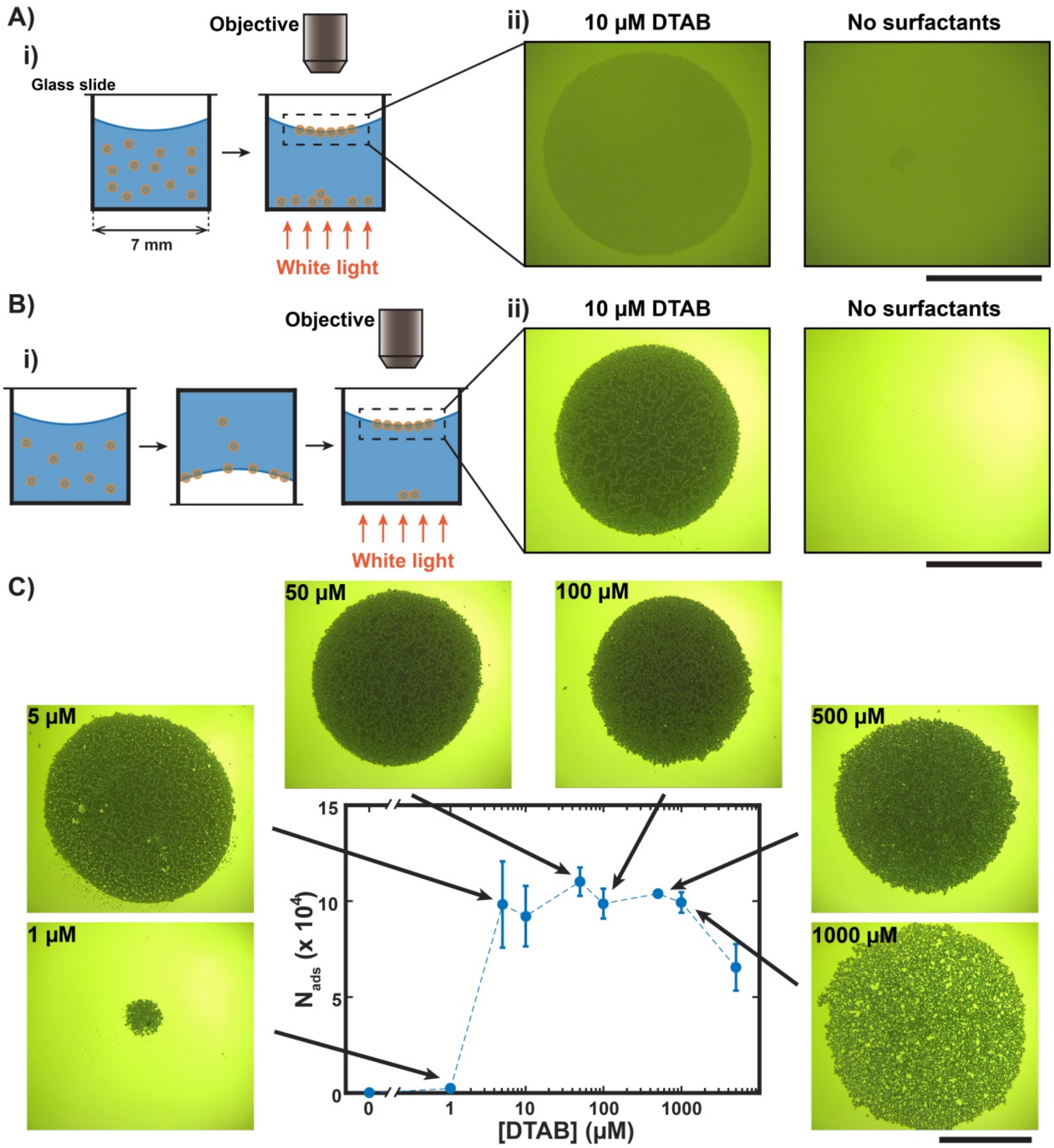

Fig. 1 Cationic surfactants (dodecyltrimethylammonium bromide, DTAB) induce the adsorption of negatively charged PS microparticles (carboxyl and sulfate surface groups, diameter: 5.1 µm) to the LG interface and mediate their subsequent self-organization in 2D colloidal assemblies. (A) The direct experiment. i) The surfactant/particle mixture is placed in a cylindrical (diameter 7 mm) sample cell made of polystyrene, which is covered with a glass slide to avoid water evaporation, and is left unmoved overnight. A 2D patch of particles is spontaneously formed at the LG interface, as observed by brightfield transmission microscopy. The rest of the particles were at the bottom of the cell due to sedimentation. ii) A 2D colloidal crystalline patch of circular shape is formed at a DTAB concentration of C_s = 10 µM and a

particle concentration of C_p = 5 mg/mL. Contrarily, no particles are adsorbed to the LG interface (and thus no 2D assembly is formed) in a surfactant-free (C_s = 0 μM, C_p = 5 mg/mL) suspension. A representative movie, recorded shortly after loading the surfactant/particle mixture in the chamber, showing the formation of the 2D crystal in the direct experiment is provided in the Supporting Information (Movie S1). (B) The inverse experiment. i) Similar to the direct experiment, the surfactant/particle mixture is placed in the sample cell, and the latter is flipped upside down so that gravity brings the particles to the LG interface. After 2 hours, the sample cell is flipped back to its original position and the LG interface is observed with brightfield transmission microscopy. ii) For C_s = 10 μM and C_p = 0.05 mg/mL, a 2D polycrystalline patch of particles is observed. On the contrary, no particle adsorption to the LG interface (and thus no 2D assembly) is observed in a surfactant-free (C_s = 0 μM, C_p = 0.05 mg/mL) suspension. Two movies showing the formation respectively of a 2D crystal and a 2D gel-like structure in the inverse experiment are provided in the Supporting Information (Movies S2 and S3) (C) The evolution of the number of particles that adsorb to the LG interface, N_{ads}, as a function of C_s, as recorded in the inverse experiment. The brightfield transmission microscopy images show the corresponding 2D colloidal assemblies. Symbols and error bars show mean values ± sd from 3 individual experiments. All scale bars are 1 mm.

Influence of surfactants on particle adsorption and interparticle interactions

We next sought to elucidate the role of surfactants in the adsorption of the suspended particles to the LG interface and their following organization into 2D interfacial structures. To this end, we kept the particle concentration constant (C_p = 0.05 mg/mL) and we varied the DTAB concentration. We measured the number of particles (N_{ads}) adsorbed at the LG interface as a function of C_s (Fig. 1C). As mentioned earlier, there was no particle adsorption for the surfactant-free dispersions. For C_s = 1 µM, only a small amount ($N_{ads} \sim 2.3\times10^3$) of particles were adsorbed to the free interface. These particles formed a small (diameter ~ 390 µm) disordered patch of roughly circular shape. Raising the DTAB concentration to C_s = 5 µM led to a dramatic increase in the number of adsorbed particles, with N_{ads} reaching a value of about 10^5. The interfacial particles formed a dense circular patch displaying a diameter of about 2.03 mm. Further increasing the DTAB concentration, in the range C_s = 50 µM – 500 µM, did not result in an increase of N_{ads}, which remained in the order of ~ 10^5 particles. Strikingly, this N_{ads} agrees very well with the total number of particles in suspension, confirming our hypothesis that, under the appropriate conditions, all suspended particles can be adsorbed to the LG interface in the inverse experiment. Although particles always formed circular patches of approximately constant diameter, the microstructure of the colloidal assemblies was dependent on C_s. For C_s = 5 – 100 µM, the microstructure varied along the radial direction of the circular patch. Starting from its center, approximately 68% of the patch area was crystalline, whereas particles positioned in the remaining region (*i.e.*, closer to the patch edge) were less ordered. For C_s = 500 µm, particles were organized in a dense but amorphous circular patch. The situation, regarding the patch microstructure, changed drastically for C_s = 1 mM. Whereas N_{ads} remained unaltered ($N_{ads} \approx 10^5$), the adsorbed particles formed a loosely packed circular patch of increased diameter of ~ 2.2 mm. Interestingly, the number of adsorbed particles decreased with further increasing DTAB concentration, reaching $N_{ads} = 6.5\times10^4$ for C_s = 5 mM.

To investigate in depth the evolution of the microstructure of the 2D colloidal assemblies as a function of surfactant concentration, we examined the central part of the patches by means of high magnification transmission microscopy (Fig. 2A and Fig. S3). We quantified the observed evolution by computing the radial distribution functions (RDF) from these images (Fig. 2B). The RDF represents the probability to find a particle at a certain center to center distance, r, from a given particle. For C_s = 1 µM, the particles were organized in a relatively dense arrangement. However, the latter was mostly disordered, showing only a few cases of particle organization in a tetragonal lattice. The lack of long-range order was confirmed by the RDF (Fig. 2B, blue curve). For C_s = 5 – 10 µM, particles were arranged in a close-packed hexagonal lattice including a few defects. The corresponding RDF revealed the long range positional order, showing clear peaks up to distances (normalized with the particle diameter D) of $r/D = 10$. This increased positional order was maintained for $r/D = 6$ for higher DTAB concentrations, up to C_s = 100 µM. For C_s = 500 µM, most of the long-range order was lost, while for $C_s \geq 1$ mM the structure was disordered, with patches adopting a 2D gel-like morphology (Fig. 1C and Fig. 2A).

Although limited by the resolution of our microscope, another interesting observation concerning the interparticle center-to-center distance, can be made. At C_s = 5 – 10 µM, where the 2D colloidal crystals with the longest range of order were formed, the distance of a given particle to its first neighbor, r_1, was slightly larger than one particle diameter. With increasing DTAB concentration, up to C_s = 100 µM where still a long-range ordered colloidal crystal occurs, r_1

decreased to about one particle diameter, *i.e.* $r_1/D \approx 1$ (inset of Fig. 2B). This decrease in interparticle distance suggests that particle-particle attractions increased. This was further confirmed by the observation that particles were in contact with further increasing C_s, leading to the formation of amorphous aggregates and the subsequent emergence of a frozen, disordered 2D structure.

These results suggest that the surfactant concentration modulates the interactions between the interfacial particles. The condition $r_1/D > 1$ corresponds to the case where interparticle repulsion dominates. Contrarily, $r_1/D \approx 1$ indicates that neighboring particles are in contact, which in turn implies that particle-particle attractions overcome repulsions. This scenario would be in agreement with repulsion being the requirement for colloidal crystallization (Movie S2), and attraction (leading to particle aggregation) being at the origin of the formation of a kinetically arrested 2D structure (Movie S3).

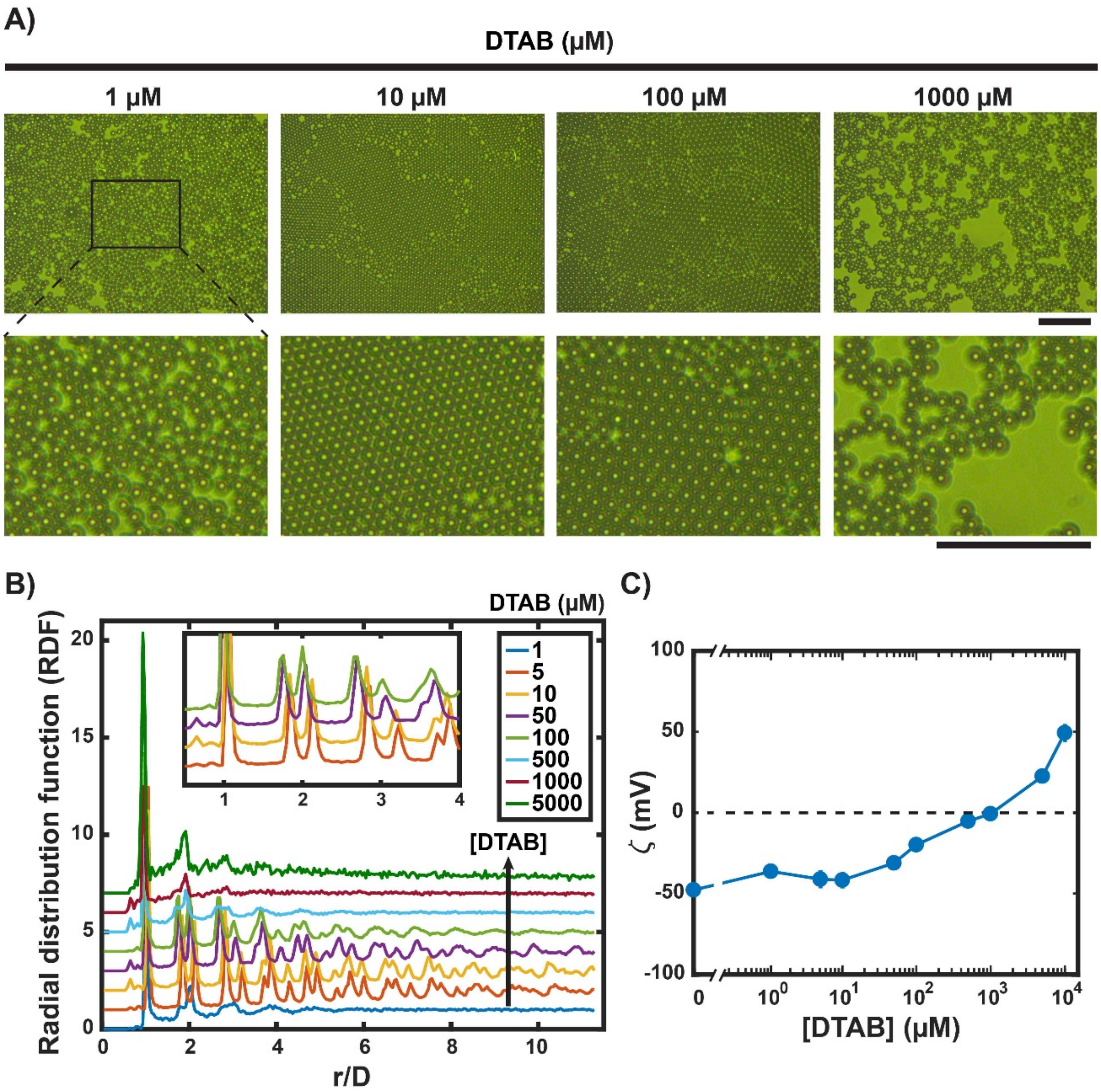

Fig. 2 The concentration of DTAB i) dictates the interactions of the PS microparticles with the LG interface, which in turn control particle adsorption and ii) affects the interactions between interfacial particles, once they are adsorbed. (A) Evolution of the microstructure of the 2D colloidal assemblies obtained with the inverse method versus C_s, as evidenced by brightfield transmission microscopy. The particle was concentration was fixed at C_p = 0.05 mg/mL. The top row shows high magnification images of the interfacial assemblies. Zoomed images of the central area of these assemblies (indicated by a black square) are shown in the bottom row. The scale bars are 50 μm. (B) The radial distribution functions (RDF) computed from the images in (A), top row; r is the interparticle distance, D is the particle diameter. The RDF are vertically offset for the ease of comparison. The inset shows a magnified view of

the first peaks of the crystal structures, revealing a shift towards shorter interparticle distances upon increasing surfactant concentration. (C) Zeta potential (ζ) measurements of mixtures of PS particles (C_p = 0.05 mg/mL) with varying concentrations of DTAB. Symbols represent mean values of six independent measurements. The error bars (standard deviation) are smaller than the symbol size.

The role of the electrostatic surface properties of the particles

With a view of addressing the validity of the above scenario, we investigated how the amount of surfactant molecules affected the electrostatic properties of particles in suspension. We measured the zeta potential (ζ) of the utilized mixtures, keeping C_p = 0.05 mg/mL and varying C_s (Fig. 2C). The PS particles displayed a negative surface potential of ζ = -50 mV, as a result of their dissociable surface groups (being mostly carboxylic acid). For DTAB concentrations up to C_s = 10 µM, ζ retained its value, indicating that in this C_s range, there was no significant surfactant adsorption on the surface of the particles. Interestingly, this exactly matches the C_s window for which the most long-ordered 2D colloidal crystals were formed (Figure 2B). With further increasing DTAB concentration, the surface potential of the particles started to decrease, assuming a values of ζ = -31 mV and ζ = -20 mV, for C_s = 50 and µM C_s = 100 µM, respectively. This finding suggests that, above C_s = 100 µM surfactants started to significantly adsorb on the particle surface, which in turn should have a direct influence on the interactions between interfacial particles. This was indeed reflected on the microstructural characteristics of the formed colloidal crystals, as evidenced by the surfactant concentration effect on the interparticle distance and the range of the positional order (Figure 2B). Further addition of DTAB molecules to the latex suspensions led to the neutralization (C_s = 0.5 – 1 mM) and then to the overcharging (C_s = 5 – 10 mM) of the particles. This is attributed to the formation of a monolayer and a bilayer of DTAB molecules on the particle surface, respectively (14). Strikingly, the neutralized particles formed kinetically arrested gel-like structures, when adsorbed at the LG interface. These results unambiguously confirm the predominance of particle-particle attractions at the free interface for C_s = 0.5 – 1 mM.

Interestingly, the overcharged (*i.e.* positively charged) particles did not significantly adsorb to the LG interface (Figure S3). This can be explained by the fact that cationic particles experienced a Coulomb repulsion from the DTAB-laden LG interface, which was also positively charged.

Such an explanation is further supported by additional experiments conducted with positively charged PS microparticles, bearing amidine groups on their surface. Our results showed that these cationic microparticles adsorbed to the pure (*i.e.* surfactant-free) air-water interface, which is considered negatively charged (18) (Figure S4).

For C_s = 5 µM – 5 mM, where substantial particle adsorption at the LG interface occurred, strongly negatively charged particles (no surfactant adsorption) formed long-range ordered crystals whereas less charged particles (partial surfactant adsorption) formed crystals with shorter range order. Neutral particles (surfactant monolayer on particle surface) formed kinetically arrested 2D structures. We can thus conclude that, there is a clear correlation between the surface potential of the particles (and thus their interactions) in the bulk and the microstructural features of the interfacial colloidal assemblies.

Effect of particle concentration on two-dimensional crystallization

We observed that, although particle adsorption to the LG interface took place and particles were negatively charged for C_s = 1 µM, no 2D colloidal crystals were formed (Fig. 2A). Interestingly, the absence of 2D crystallization corresponded to the case where only a few ($N_{ads} \approx 2.3\times10^3$) particles were adsorbed to the LG interface (Fig. 1C). This led us to hypothesize that colloidal crystallization could occur at this low surfactant concentration, provided that an adequate number of interfacial particles is available. To assess the validity of this hypothesis, we explored the influence of particle concentration, at C_s = 1 µM, on the number of particles adsorbed to the LG interface (Fig. 3A) and the microstructural characteristics of the resulting assemblies (Fig. 3B and Figure S5). For very dilute suspensions (C_p = 0.01 mg/mL), almost no particles were present at the LG interface. A gradual increase in N_{ads} was observed with increasing particle concentration from C_p = 0.05 mg/mL to C_p = 1 mg/mL, with the respective values being $N_{ads} = 2.3\times10^3$ and $N_{ads} = 8\times10^3$. Further raising C_p to 5 mg/mL resulted in a more drastic increase in N_{ads}, which assumed a value of 2.3×10^4. Interestingly, this clear tendency of increasing the number of particles adsorbed to the LG interface with increasing particle concentration in the bulk (*i.e.* C_p) is in agreement with our finding presented earlier, that surfactants did not adsorb on the particles at such low C_s.

The amount of interfacial particles had a profound effect on the microstructure of the 2D colloidal assemblies, as demonstrated by the corresponding RDF shown in Fig. 3B (microscopy images are shown in Figure S5). For the lowest particle concentration (C_p = 0.01 mg/mL) and hence the minimum number of adsorbed particles, the resulting structure was close-packed but lacked any long-range order. For C_p = 0.05 – 0.5 mg/mL, the degree of order of the interfacial colloidal rafts clearly increased, as shown by the emergence of sharp peaks at r/D = 2 and r/D =3 in the RDF. Interestingly, further increasing the number of adsorbed particles by using more concentrated suspensions drastically improved the degree of two-dimensional order, which extended to distances r/D = 7 and r/D = 9 for respectively C_p = 1 mg/mL and C_p = 5 mg/mL, corresponding to $N_{ads} = 8\times10^3$ and $N_{ads} = 2.3\times10^4$, respectively. A similar dependence of the particle behavior at the LG interface on particle concentration was observed at fixed C_s = 10 µM (Figure S6). All these results clearly demonstrate that, when an adequate number of particles was adsorbed to the LG interface, colloidal crystals emerged at the interface. Furthermore, the range of crystalline order of these interfacial assemblies increased with increasing the surface concentration of the particles, which was achieved by simply raising C_p.

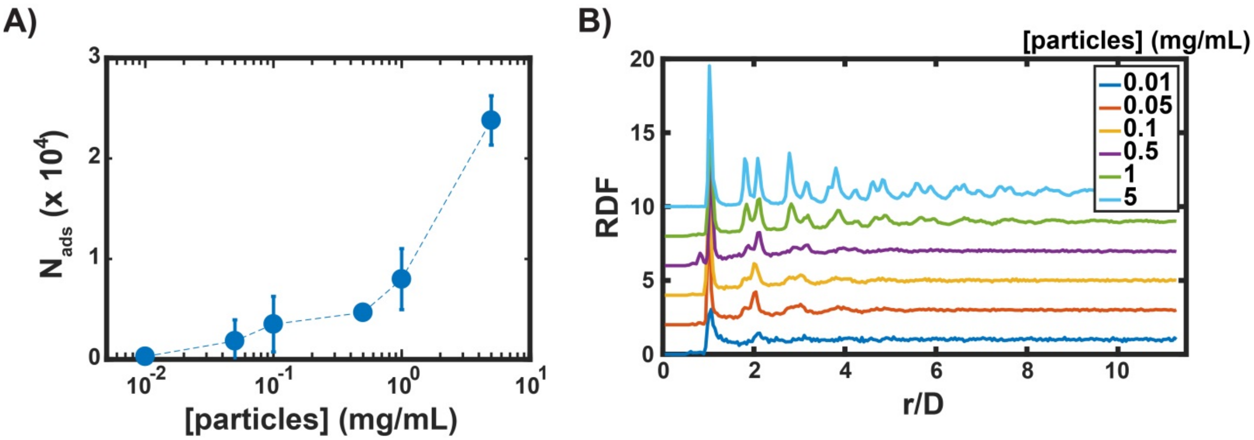

Fig. 3 Raising the particle concentration in suspension increases the number of particles adsorbed to the LG interface and promotes the tendency to 2D colloidal crystallization. (A) The number of adsorbed particles (N_{ads}) at the LG interface at (C_s = 1 µM), versus particle concentration (C_p), as obtained from the inverse experiment. Symbols and error bars show mean values ± standard deviations from 3 individual experiments. (B) The radial distribution functions (RDF) computed from the images (Fig S5) of the

colloidal assemblies formed at different C_p (C_s = 1 µM) versus particle concentration; r is the interparticle distance, D is the particle diameter. The RDF are vertically offset for clarity.

Comparison between direct and inverse experiments

As mentioned earlier (Fig. 1), the adsorption and the self-organization behavior of the particles at the LG interface were qualitatively similar for the direct and the inverse experiments. It is interesting at this point to compare the microstructural properties of the interfacial colloidal assemblies resulting from these two methods. We begin by discussing in detail the assemblies formed in the direct experiments using a fixed particle concentration (C_p = 5 mg/mL) and varying C_s. We utilized white light-based confocal microscopy to visualize the structure of the assemblies with higher lateral resolution, as well as to quantitatively map the vertical positioning of single particles at the LG interface, as discussed later in more detail. The height images corresponding to particle monolayers formed at different surfactant concentrations are shown in Fig. 4A, and the respective RDF are presented in Fig. 4B. Hexagonally packed crystallites made up polycrystalline patches for all DTAB concentrations in the range C_s = 1 – 100 µM. However, the long-range order of the interfacial structures was dependent on the exact value of C_s. Well-ordered crystals for distances up to r/D = 9 were observed for C_s = 1 – 50 µM, whereas the range of order considerably decreased for C_s = 100 – 500 µM. Largely disordered particle monolayers were observed for the two highest DTAB concentrations examined, C_s = 1 mM and C_s = 5 mM respectively. These results are generally in accordance to the ones obtained with the inverse experiment, except for the the extreme cases of very low and very high C_s. In the direct experiments, well-ordered crystals were obtained for C_s = 1 µM, whereas in the inverse experiments we observed the formation of an amorphous close-packed colloidal patch. This dissimilarity can be explained by the difference in the number of adsorbed particles, which was larger in the direct experiment (Fig. S7); increasing the number of interfacial particles increases the tendency for particles to crystallize (Fig. 3). For C_s = 5 mM, the observed differences may be attributed to the different mechanisms that transport particles at the free interface. Gravity was able to bring both particles and large aggregates to the LG interface in the direct experiments. Contrarily, aggregate transport to the interface due to convection might have been limited in the direct experiment, explaining the very low number of only single particles at the LG interface (Fig. 4A).

The results from the direct and inverse experiments indicates that, a DTAB concentration in the order of µM induced the adsorption of particles to the free interface, regardless of the exact particle concentration in the bulk. The role of the latter was to define the microstructural characteristics of the formed 2D assemblies. For the inverse experiment, where the mechanism responsible for transporting particles to the interface is well controlled, increasing the particle concentration in-suspension led to larger number of interfacial particles. This in turn increased the tendency of the adsorbed particles to assemble in ordered close-packed 2D crystals.

Elucidating the role of particle contact angle at the liquid-gas interface

From the height images of the particles at the LG interface (Fig. 4A), we measured the fraction (P) of the diameter of each particle that was exposed to the air phase. We were then able to calculate the contact angle (θ) that each individual particle makes with the air-water interface, $\theta = arcos(D\text{-}2P)/D$ (Figure S8). To our knowledge, this is the first time that confocal microscopy was used to measure *in-situ* the contact angle of a microparticle at the LG interface. The evolution of the particle contact angle as a function of C_s is shown in Fig. 4C. Note that the θ values depicted are the average values from about 10^3 individual particles that were typically contained in a single image (for details see Figure S8). Interestingly, the contact angle that the particles made with the LG interface did not depend on the DTAB concentration for $C_s = 0 – 1$ mM, assuming a value of $\theta \approx 30^o$. Note that the θ corresponding to $C_s = 0$ mM (data point indicated with red color) is the angle that the very limited number of adsorbed particles formed with the LG interface. Since the vast majority of particles were not adsorbed to the interface in these surfactant-free samples, we can conclude that the actual θ value is 0^o. Moreover, for $C_s = 5$ mM, only a few particles were adsorbed to the interface. These particles displayed contact angle clearly smaller than 30^o, which however could not be evaluated since the P values were too small to be measured (Figure 4B).

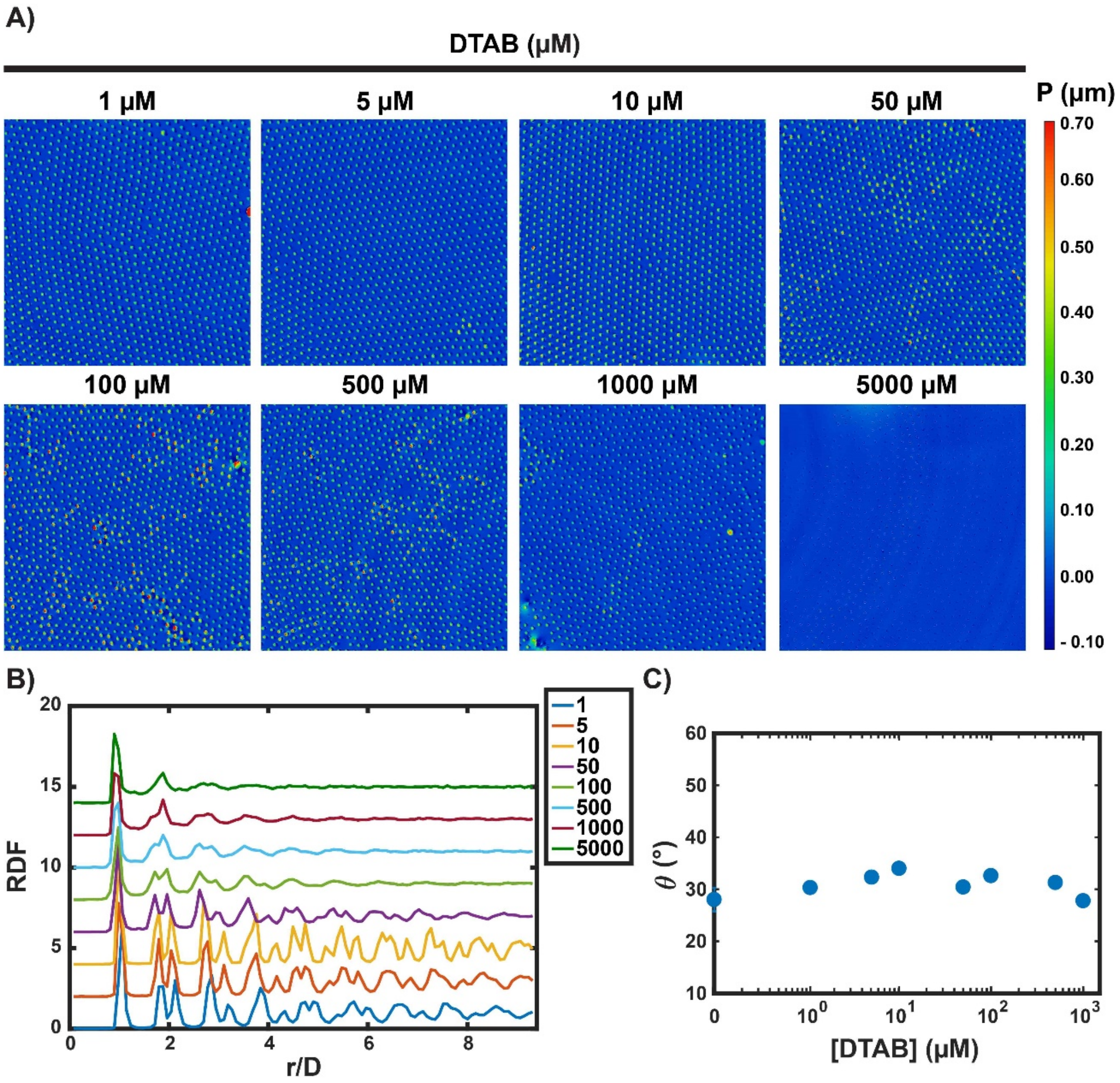

Fig. 4 *In-situ* confocal microscopy experiments reveal the exact positioning in three-dimensions of the PS microparticles at the LG interface (A) Height images of the interfacial particle assemblies obtained by varying C_s (C_p = 5 mg/mL) *via* the direct method. *P* is the fraction of the diameter of the particle that is exposed to the air phase. (B) The radial distribution functions (RDF) corresponding to the height images shown in (A). The RDF are vertically offset for the ease of comparison. (C) The average values of the contact angle that each PS particles forms with the LG interface, as a function of C_s. The value at C_s = 0 μM (red point) corresponds to only a few particles which were present at the LG interface (see main text). At 5 mM the point is missing because the images are not analyzable due to the very small *P* values. The details of these measurements are included in the Supporting Information (Figure S8).

A number of important conclusions for the C_s = 1 μM – 1 mM range, where crystallization was observed, might be drawn from the above results. First, the fact that θ remains unchanged indicates that the wetting properties of the microparticles in this C_s range remain unaltered as well. We could assume that this high wettability is due to the inherent particle properties (hydrophilic surface due to the presence of carboxyl and sulphate groups), and it is not affected by the presence of surfactants. Significant surfactant adsorption for C_s = 1 μM – 100 μM was excluded on the basis of zeta potential measurements (Fig. 2C) which indicated that the surface potential of the particles did not change with C_s in this range. In addition, although surfactants adsorbed onto the particles for C_s = 0.5 mM – 1 mM, and made them electrostatically neutral, there was no effect on the average θ values. Second, a contact angle of $\theta \approx 30^o$ corresponds to a linear immersion fraction $P/D \approx 6\%$, implying that almost the whole PS microparticle is immersed in the aqueous phase. Williams and Berg have shown that at such low immersion fractions, the effective Hamaker constant describing the van der Waals interaction between two PS particles adsorbed at the air-water interface is almost equal to the Hamaker constant for PS particles that are suspended in (bulk) water (15). We can therefore assume that, for our system, the classical DLVO description (originally developed for interparticle interactions in the bulk) can account for the particle-particle interactions at the interface. On the contrary, for C_s > 1 mM, surfactants significantly adsorb onto the microparticles and they consecutively modify both their surface charge and wettability, and in turn their interactions with the LG interface.

Overall, our *in-situ* confocal microscopy experiments indicated that, for the DTAB concentration range where interfacial crystals were formed, the contact angle of the particles assumed a constant value of about 30^o. This result implies that the evolution of the order of the interfacial particle monolayers with C_s is not due to changes in particle wettability, as observed in other colloid/surfactant mixtures (Maestro, Mugele?, Binks?). Instead, it is the result of the DLVO interactions between the particles in the bulk, which can describe well the interactions between the almost fully immersed (in water) interfacial particles.

Proposed explanation and the phase diagram of the interfacial particle self-organization

We here summarize our findings and propose an explanation for the observed phenomena. First, we have discovered that an amount of DTAB in the order of 1 μM (*i.e.*, four orders of magnitude lower than the CMC = 13.4 mM(14)) induced the adsorption of the PS microspheres to the LG interface. Dispersions in pure water (C_s = 0 μM) or dispersions with $C_s \geq 5$ mM, showed no (direct experiment) or decreased (inverse experiment) particle adsorption to the free interface, respectively. Interestingly, we observed a similar behavior when a more hydrophobic cationic surfactant, hexadecyltrimethylammonium bromide (CTAB), was added to the microparticle suspensions. We obtained a curve of particle adsorption at the LG interface similar to the one with DTAB, but shifted to a lower C_s (Fig. S9). We attribute this to the higher surface activity of CTAB (CMC = 0.92 mM(14)), which implies that a lower amount of surfactant was enough to efficiently decrease the adsorption barrier. Interestingly, from 50 μM (neutral particles as measured from ζ potential, see Fig. S10), very few particles adsorb to the LG interface. Similar to the DTAB case, 2D crystals were also obtained with CTAB, even though the latter displayed a decreased range of positional order (Fig. S9). Contact angle discussion here?

Contrarily, the presence of anionic or neutral surfactants did not lead to particle adsorption. It is well known that ionic surfactants adsorb onto oppositely charged particles and they in turn induce their adsorption to fluid interfaces, by increasing the hydrophobicity of the particles (REFS). However, our results are not in accordance with such a mechanism. As we demonstrate by zeta potential measurements in the bulk (Fig. 2C) and *in-situ* measurements of the contact angles that the particles formed with the LG interface (Fig. 4C and Fig. S10), our particles were adsorbed to the free interface at C_s where their wetting and the electrostatic properties were not influenced by the presence of surfactants. At such low C_s, instead of adsorbing to the particle/water interface, surfactants preferably populate the LG interface. Their surface concentrations are low, as indicated from the fact that air-water interfacial tensions are close to that of pure water (19). We postulate that the low amount of adsorbed cationic surfactants is adequate to reduce the total energy barrier between adsorbing particles and the LG interface, which is the result of the repulsive van der Waals and electrostatic interactions between them (15). An effect qualitatively similar to the surfactant-driven effect described here has been reported in similar PS latex suspensions, where the addition of electrolytes resulted in enhanced particle adsorption to the air-water interface (15–17). The height of the adsorption barrier, described by the classical DLVO theory after considering the effects of the solvation zone around the particles and the air-water interfacial regions, was decreased with increasing the ionic strength of the suspension (17). We believe that the surfactant cations have an action similar to electrolytes, however they are more effective than the latter as they are preferentially located (*i.e.* adsorbed) at the LG interface, acting effectively as ‘super-salts’.

We observed that, once adsorbed, the interfacial microparticles did not leave the free interface. This was due to the reduction of the total surface energy associated with the transport of a suspended particle from the bulk to the partially wetted state at the interface, resulting in the ‘capillary trapping’ of the particle at the interface (20), in agreement with earlier work (21). The ‘trapped’ particles were then spontaneously self-organized in various two-dimensional structures, ranging from small, disordered close-packed assemblies to large polycrystalline patches to gels.

Based on our experimental observations, we constructed a phase diagram comprising of the two experimental parameters dictating the phase behavior of this 2D colloidal system, namely the surfactant and the particle concentration (Fig. 5). Both C_s and C_p define the balance of attractive and repulsive interactions between interfacial particles, which ultimately dictates the microstructure of the colloidal assemblies. We first note that, in our experimental system, a mechanism responsible for locally increasing the surface concentration of (adsorbed) particles is always at work, due to the wetting properties of the sample cell. The contact angle of our surfactant/particle aqueous mixtures on the walls of our plastic cell was always less than 90^o, resulting in a concave meniscus (Fig. S11). This shape caused interfacial particles to always move toward the center of the LG interface due to the action of gravity.

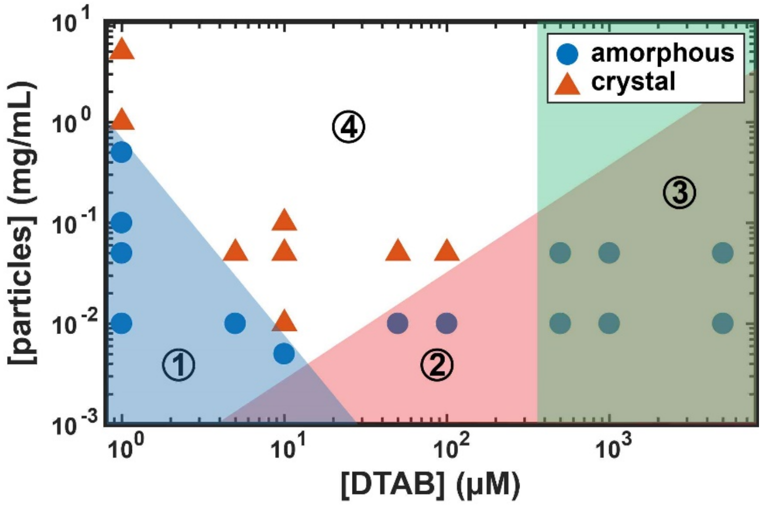

Fig. 5 The experimental phase diagram describing the behavior of the adsorbed PS particles at the LG interface. The varied experimental parameters are respectively the PS particle concentration (C_p) and the DTAB concentration (C_s).

On the one hand, for a given C_p and for 1 µM ≤ C_s ≤ 100 µM, the particles remained strongly negatively charged (Fig. 2C) and the role of surfactants was to finely tune the interparticle distance. This occurred for $C_s \geq 50$ µm, where surfactant addition screened the electrostatic repulsion and led to shorter particle-particle spacing. Therefore, given the linear immersion fraction, electrostatic repulsions dominated, resulting in the formation of kinetically arrested structures. For 0.5 mM ≤ C_s ≤ 1 mM, on the contrary, particles were almost neutralized; therefore the attractive van der Waals interaction is expected to dominate. On the other hand, for a constant C_s, we observed that raising the C_p led to an increased number of interfacial particles (Fig. 3A), resulting in turn in a general tendency for more ordered structures (Fig. 3B). We believe that this is due to a ‘collected sinking effect’, leading to closer particle bounding at fluid interfaces when the number of interfacial particles increases (22). In the latter case, the local curvature of the interface decreases and particles move to the lower part of the meniscus1., which consequently leads to enhanced particle-particle attractions.

I think we should add a small paragraph contrasting our work with the infamous works in the field, especially Pieranski and Onoda; the main points of this are to make sure that we mention somewhere these landmark works, and to clearly distinguish our work. Interestingly, after the first report on the formation of interfacial colloidal crystals [Pieransky], few works studied the organization of particles coming from bulk solution at the air-water interface addressing either the formation of ordered clusters as a function of particles size at fixed salt concentration [Onoda], or the adsorption rate and subsequent aggregation varying the salt concentration [Williams and Berg]. **DON'T FORGET THE PROMOTERS WORK (HYDROPHOBIC SALTS) IN NANOLETTERS** Afterward the majority of studies that address the aggregation state of particles monolayers at the air-water interface exploited the direct adsorption of particles at the interface by means of spreading the particles dispersed in an immiscible and volatile solvent [refs Vermant, Aveyard, etc... for properties. Vogel, etc… for materials]. As far as I know, surfactants were added to control the aggregation [Vermant Langmuir 2006] and particle-particle interactions (at oil-water interface) [Vermant Langmuir 2008] only after the monolayer formation. It was reported that the addition of surfactants induced aggregation of the previously ordered monolayer.

Application of the surfactant-driven mechanism for the 2D crystallization of silica particles

We have so far established that the 2D crystallization of the PS microparticles at the LG interface took place at C_s where there was negligible surfactant adsorption onto the particles. This suggested that the role of the surfactants was mainly to reduce the barrier for adsorption, and secondarily to modulate the repulsive interactions between adsorbed particles. We hence hypothesized that this surfactant-driven phenomenon should be insensitive to the exact physicochemical properties of the particles. This in turn led us to hypothesize that this crystallization methodology should be applicable to other types of anionic particles. To test this hypothesis and challenge the breadth of applicability of this method, we mixed hydrophilic silica particles (diameter: 4.62 µm, silanol surface groups) with DTAB. In the case of surfactant-free dispersions, we observed no particle adsorption at the air-water interface (Figure S12). On the contrary, 2D crystals were obtained when DTAB was added in suspension, at the same concentration (C_s = 10 µM) as in the case of PS particles. Interestingly, the entire colloidal assembly was crystalline in the case of silica particles, a feature never observed in the case of PS particles. Additionally, due to their higher density, the silica particles quickly accumulated at the center of the LG interface, leading to a significantly faster crystallization kinetics compared to the case of the PS particles of similar size (Movie S4). We believe that those aspects are a direct consequence of the “collective sinking effect”(22), which was more pronounced in the case of silica microparticles due to their higher density (1.85 g/cm^3) compared to PS (1.06 g/cm^3). Finally we observed that the crystalline silica domains were generally composed of a higher number of particles compared to the PS case, presumably due to the lower size polydispersity of the former system. Our findings may open the way for the development of a straightforward, efficient and cost-effective methodology of engineering 2D crystals from diverse colloidal suspensions of anionic particles, utilizing cationic surfactants at exceptionally low concentrations.

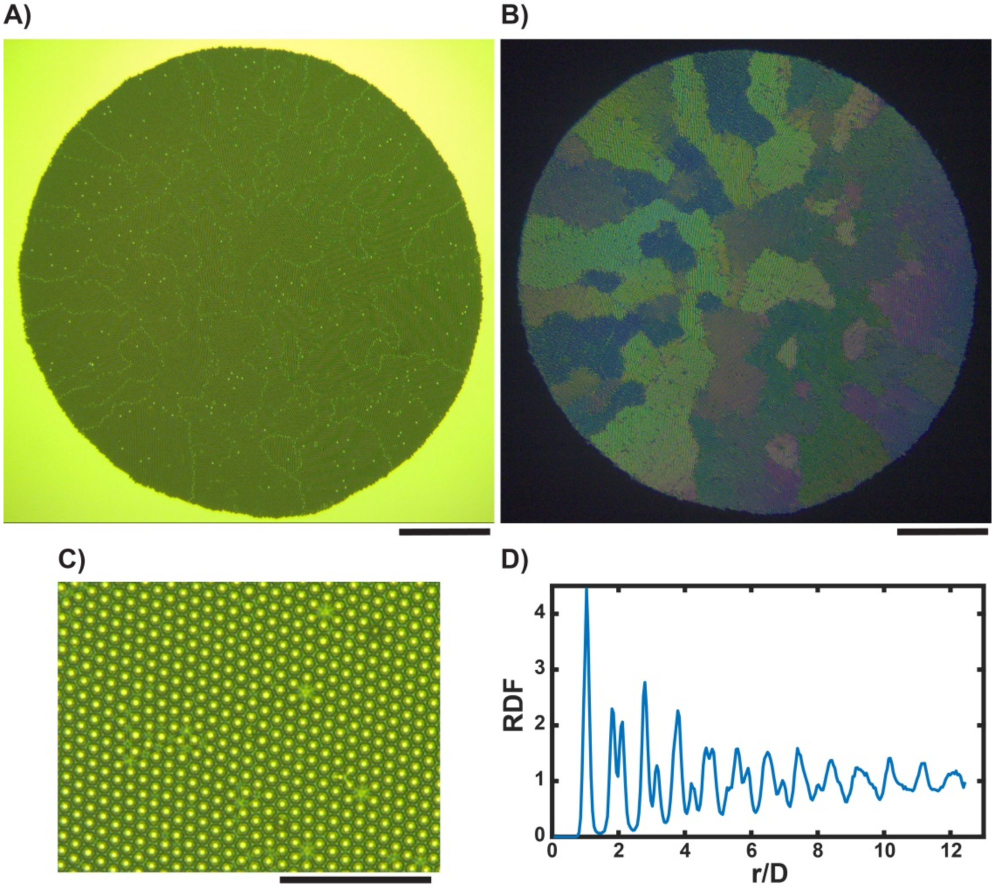

Fig. 6. Cationic surfactants (DTAB) induce the adsorption and the subsequent crystallization of negatively charged silica microparticles (diameter: 4.62 μm) at the LG interface. A) Transmission microscopy image of a 2D polycrystalline patch (diameter 1.55 mm) obtained with the inverse method, using a sample with of C_s = 10 μM and C_p = 0.05 mg/mL. The scale bar is 300 μm. B) Reflection image of the same sample as in (A) obtained using white light illumination from the side of the chamber. The

observed colors are the result of selective reflection from the different crystalline domains. The scale bar is 300 µm. C) High magnification image of the central region of the aggregate in (A). The scale bar is 50 µm. D) The RDF computed from an area of 250 µm x 190 µm of the silica colloidal crystal.

Conclusions

To be added soon…

Materials and methods

Materials. Ultrapure water (resistivity 18.2 MΩ•cm) was used for all experiments. The suspensions of negatively charged polystyrene particles (diameter: 5.1 µm) bearing sulphate and a high density of carboxyl functional groups on their surface, were purchased from Life Technologies (CML latex, catalogue number: C37255). Although the suspensions were designated as surfactant-free, we followed a washing procedure that was found to be essential for obtaining reproducible results. A suspension of the particles at C_p = 10 mg/mL underwent typically five to six centrifugation cycles and, each time the supernatant liquid was exchanged with ultrapure water. Prior to each experiment each particle suspension was mixed (2 min), sonicated in an ultrasound bath (2 min), and mixed for another minute. Dodecyltrimethylammonium bromide (DTAB, purity ≥ 98%, Sigma-Aldrich), hexadecyltrimethylammonium bromide (CTAB, purity ≥ 99%, Sigma-Aldrich), sodium dodecyl sulfate (SDS, purity ≥ 99%, Fluka), and triethoxy monooctylether (C8E3) were used as received.

Sample preparation. Two methods were used for preparing the surfactant/particle mixtures. In the case of the inverse method, the proper amounts of water, concentrated particle suspension, and concentrated surfactant solution were added in this order in the cylindrical well (polystyrene, diameter 7 mm, Nunc Lab-Tek). Then the well was first inverted to an upside-down position, with the air-water interface being underneath the particle/surfactant mixture. The sample was left in this position for two hours, so that the particles (polystyrene density: 1.06 g/cm^3) accumulate at the air/water interface due to gravity. Then the well was turned upside down once again, with the air-water interface now being on top of the liquid, and was placed on the microscope stage where it was left unmoved overnight.

In the case of the direct method, the proper amounts of water, concentrated surfactant solution, and concentrated particle suspension were added in this order in an Eppendorf tube. After mixing with a micropipette (Eppendorf), the suspension was loaded in a cylindrical well, and the well was placed overnight on the microscope stage. I need to crosscheck the sonication/vortexing details

Image acquisition and analysis. All microscope images other than the height images shown in Fig. 4A, were acquired using a home-built upright microscope, which could operate both in transmission and reflected mode. The microscope mainly consisted of a 12X Zoom Lens System (Navitar), the appropriate microscope objective (a 20X, *NA* = 0.42 and a 5X, *NA* = 0.14 for respectively low and high magnification, both from Mitutoyo) and an XYZ translation stage, on which the sample cell was placed. White light illumination was provided by a flexible light guide coupled to a cold light source (KL 2500 LED, Schott). The white light was either coupled directly to the tube system (*via* a side port) for reflection imaging, or was brought from the bottom of the sample cell after passing through a diffuser and a mirror for transmission imaging. A color CCD camera (Basler acA1600-20uc, resolution 1626 pixels × 1234 pixels, 12 bits) was used for image acquisition.

Quantitative analysis of the images was carried out using the *ImageJ* software. From the high magnification images of Fig. ?? (containing between 1000 and 1800 particles), the centre of each particle in the image was set with the "find maxima" process. Knowing the positional data of the particles enabled to calculate the radial distribution function, which describes the probability of finding a particle at a (center to center) distance *r* away from a given reference particle, using the "radial distribution function" macro.

The number of particles in each patch was computed knowing the exact number of particles in the corresponding high magnification picture, and the patch area obtained fitting the patch shape with an ellipse. The particle density was assumed to be the same in the whole patch.

Confocal microscopy and calculation of the particle contact angle. Fast confocal reflection microscopy at the air/water interface was conducted using…

Each acquired image, containing around 1000 particles, was first levelled using the *μsoft* software (Nanofocus) to correct for the curvature of the LG interface. and analysed with *Gwyddion* software. A threshold by height was applied, and a distribution of the maximum fraction (P) of the diameter of the particle outside the water phase of each particle in the image was obtained. The contact angle (θ) was calculated with the following formula:

$$\cos\theta = \frac{|P - R|}{R}$$

where R is the particle radius. Further analysis was carried out with *MATLAB* software: the distribution was fitted with a Gaussian function to extract the centre of the peak and the standard deviation. In case of a double peak in the contact angle distribution, a double Gaussian function was used for fitting, and the obtained contact angles were averaged, weighted by the intensity of each peak. Mention that a much higher volume was used for those experiments discussion about contact angle distribution: DOI: 10.1021/la5040195

Measurement of the ζ-potential of the particles. Mixtures at the required particle and surfactant concentration were loaded in Eppendorf tubes, and were vortexed (1 min) and sonicated (1 min) in an ultrasound bath prior to being loaded in plastic capillary cells (DTS1070, Malvern Instruments) using a plastic syringe. The particle surface potential was measured utilizing a Zetasizer Nano-ZS (Malvern Instruments). All experiments were performed at 22 °C. Each measurement lasted 120 s and was repeated six times.

ACKNOWLEDGEMENTS

The authors would like to thank Benoit Loppinet for his insightful suggestion of using confocal microscopy to measure the contact angle of microparticles at the air-water interface. MA acknowledges funding from the European Commission (FP7-PEOPLE-2013-IEF/Project 624806 “DIOPTRA”). Other funding sources to be mentioned here?

Author contributions

MA and AB discovered the effect of surfactant-mediated crystallization of microparticles at the LG interface. MA designed the research plan and coordinated the work together with DB. MA conducted all the direct experiments; JV performed all the inverse experiments. MA and AB carried out the confocal microscopy experiments; JV calculated the particle contact angles. JV, MA and DB analyzed all data with the assistance of GKA, HJB and BPB. MA and DB wrote the paper with contributions from all authors.

Significance statement (not ready yet, just kept an old piece of text that I had written)

The scientific relevance of our results is that they shed new light on the interactions between a colloidal particle and the air-water interface, which remain poorly understood (7). We show that these interactions can be modified by the addition of surfactants, which effectively enable particles to overcome the electrostatic barrier for adsorption. Furthermore, by varying the surfactant and particle concentration, the interactions between the adsorbed particles can be finely tuned, thus enabling us to precisely control the microstructure of the formed particle monolayer. It is therefore foreseen that the acquired knowledge will provide useful guidelines for the design of functional two-dimensional materials that can be created via self-assembly (23) in a simple and cost-effective way.

References

1. McGorty R, Fung J, Kaz D, Manoharan VN (2010) Colloidal self-assembly at an interface. *Mater Today* 13(6):34–42.
2. Velev OD, Gupta S (2009) Materials Fabricated by Micro- and Nanoparticle Assembly - The Challenging Path from Science to Engineering. *Adv Mater* 21(19):1897–1905.
3. Vogel N, Retsch M, Fustin C-A, del Campo A, Jonas U (2015) Advances in Colloidal Assembly: The Design of Structure and Hierarchy in Two and Three Dimensions. *Chem Rev* 115(13):6265–6311.
4. Zahn K, Méndez-Alcaraz JM, Maret G (1997) Hydrodynamic Interactions May Enhance the Self-Diffusion of Colloidal Particles. *Phys Rev Lett* 79(1):175–178.
5. Edel JB, Kornyshev AA, Urbakh M (2013) Self-Assembly of Nanoparticle Arrays for Use as Mirrors, Sensors, and Antennas. *ACS Nano* 7(11):9526–9532.
6. Boniello G, et al. (2015) Brownian diffusion of a partially wetted colloid. *Nat Mater* 14(9):908–911.
7. Garbin V, Crocker JC, Stebe KJ (2012) Nanoparticles at fluid interfaces: Exploiting capping ligands to control adsorption, stability and dynamics. *J Colloid Interface Sci* 387(1):1–11.

8. Aveyard R, Clint JH, Nees D, Paunov VN (2000) Compression and Structure of Monolayers of Charged Latex Particles at Air/Water and Octane/Water Interfaces. *Langmuir* 16(4):1969–1979.

9. Maestro A, Guzmán E, Ortega F, Rubio RG (2014) Contact angle of micro- and nanoparticles at fluid interfaces. *Curr Opin Colloid Interface Sci* 19(4):355–367.

10. Maestro A, et al. (2012) Wettability of silicananoparticle–surfactant nanocomposite interfacial layers. *Soft Matter* 8(3):837–843.

11. Binks BP, Kirkland M, Rodrigues JA (2008) Origin of stabilisation of aqueous foams in nanoparticle–surfactant mixtures. *Soft Matter* 4(12):2373.

12. Binks BP, Rodrigues JA (2007) Double inversion of emulsions by using nanoparticles and a di-chain surfactant. *Angew Chem Int Ed Engl* 46(28):5389–92.

13. Anyfantakis M, Baigl D (2014) Dynamic Photocontrol of the Coffee-Ring Effect with Optically Tunable Particle Stickiness. *Angew Chem Int Ed Engl* 53(51):14077–14081.

14. Anyfantakis M, Geng Z, Morel M, Rudiuk S, Baigl D (2015) Modulation of the Coffee-Ring Effect in Particle/Surfactant Mixtures: the Importance of Particle–Interface Interactions. *Langmuir* 31(14):4113–4120.

15. Williams DF, Berg JC (1992) The aggregation of colloidal particles at the air—water interface. *J Colloid Interface Sci* 152(1):218–229.

16. Abdel-Fattah AI, El-Genk MS (1998) Sorption of Hydrophobic, Negatively Charged Microspheres onto a Stagnant Air/Water Interface. *J Colloid Interface Sci* 202(2):417–429.

17. Abdel-Fattah AI, El-Genk MS (1998) On colloidal particle sorption onto a stagnant air–water interface. *Adv Colloid Interface Sci* 78(3):237–266.

18. Mishra H, et al. (2012) Bronsted basicity of the air-water interface. *Proc Natl Acad Sci* 109(46):18679–18683.

19. Ritacco H, Cagna A, Langevin D (2006) Oscillating bubble measurements of the compression viscoelasticity of mixed surfactant–polyelectrolyte surface layers. *Colloids*

Surfaces A Physicochem Eng Asp 282–283:203–209.

20. Binks BP (2002) Particles as surfactants—similarities and differences. *Curr Opin Colloid Interface Sci* 7(1–2):21–41.

21. Pieranski P (1980) Two-Dimensional Interfacial Colloidal Crystals. *Phys Rev Lett* 45(7):569–572.

22. Lee D-G, Cicuta P, Vella D (2017) Self-assembly of repulsive interfacial particles via collective sinking. *Soft Matter* 13(1):212–221.

23. Grzelczak M, Vermant J, Furst EM, Liz-Marzán LM (2010) Directed Self-Assembly of Nanoparticles. *ACS Nano* 4(7):3591–3605.

List of S Figures and Movies

Fig. S1: PS/SDS (inverse expt, 0.05 mg/mL)

Fig. S2: PS/C8E3 (inverse expt, 0.05 mg/mL)

Fig. S3: as Fig. 2A, but show all Cs examined

Fig. S4: AMI/pure water

Fig. S5: microscope images corresponding to Fig. 3

Fig. S6: similar to Fig.3, but with Cs = 10 uM

Fig. S7: (Nads vs. Cs + image for 1 uM) x 2, one for inverse and the other for direct expt

Fig. S8: a figure about particle contact angle: a schematic showing P, and we will see what else

Fig. S9: Nads vs. Cs for PS/CTAB + microscope images

Fig. S10: PS/CTAB continuation: zeta and theta (confocal) results

Fig. S11: contact angles on NUNC plus calculated meniscus shapes

Fig. S12: silica/DTAB images

Movie S1: direct experiment, 1 mg/mL, 5 uM (I have the data, so I can make this if we agree)

Movie S2: inverse expt, 0.05 mg/mL, 10 uM

Movie S3: same as S2 but with 1 mM

Movie S4: silica crystallization